# Scaling of earthquake models with inhomogeneous stress dissipation

Rachele Dominguez*
*Department of Physics, Randolph-Macon College, Ashland, Virginia 23005, USA*

Kristy Tiampo
*Department of Earth Sciences, University of Western Ontario, London, Ontario, Canada N6A 5B7*

C. A. Serino
*Department of Physics, Boston University, Boston, Massachusetts 02215, USA*

W. Klein
*Department of Physics and Center for Computational Science, Boston University, Boston, Massachusetts 02215, USA*

(Received 19 January 2011; revised manuscript received 28 August 2012; published 15 February 2013)

Natural earthquake fault systems are highly nonhomogeneous. The inhomogeneities occur because the earth is made of a variety of materials which hold and dissipate stress differently. In this work, we study scaling in earthquake fault models which are variations of the Olami-Feder-Christensen and Rundle-Jackson-Brown models. We use the scaling to explore the effect of spatial inhomogeneities due to damage and inhomogeneous stress dissipation in the earthquake-fault-like systems when the stress transfer range is long, but not necessarily longer than the length scale associated with the inhomogeneities of the system. We find that the scaling depends not only on the amount of damage, but also on the spatial distribution of that damage.

DOI: 10.1103/PhysRevE.87.022809 PACS number(s): 89.90.+n, 91.30.Bi, 91.30.Ab, 91.30.Px

## I. INTRODUCTION

A recent paper [1] shows that introducing inhomogeneities or damage into simple models of earthquake fault systems can account for several features associated with Gutenberg-Richter (GR) scaling. In this approach, the event size scaling relies on a spinodal critical point [2], in contrast to other proposed sources of GR scaling such as self-organized criticality [3,4] or the scale invariance of the individual fault length scales [5,6].

In Ref. [1], damage was distributed randomly in the models. In real faults, the spatial arrangement of fault inhomogeneities is dependent on the geologic history of the fault. Because this history is typically quite complex, the spatial distribution of the various inhomogeneities occurs on many length scales. One way that the inhomogeneous nature of fault systems manifests itself is in the spatial patterns which emerge in seismicity graphs [7,8].

Despite their inhomogeneous nature, real faults are often modeled as spatially homogeneous systems. One argument for this approach is that earthquake faults have long-range stress transfer [9], and if this range is longer than the length scales associated with the inhomogeneities of the system, the dynamics of the system may be unaffected by the inhomogeneities. However, it is not clear that this is the case. Consequently it is important to investigate the situation in which the stress transfer range is comparable to or less than the length scales associated with the damage or stress dissipation inhomogeneities. A goal of this work is to further test the approach to GR scaling developed in Ref. [1] against the inclusion of spatially inhomogeneous damage.

In this work, we study scaling in cellular automaton models of earthquake faults. We use a variation of a model introduced initially by Rundle, Jackson, and Brown (RJB) and reintroduced independently by Olami, Feder, and Christensen (OFC) to explore the effect of spatial inhomogeneities in earthquake-fault-like systems when stress transfer ranges are long, but not necessarily longer than the length scales associated with the inhomogeneities of the system [10,11]. For long-range stress transfer without inhomogeneities, as well as randomly distributed inhomogeneities [1], such models have been found to produce scaling similar to GR scaling found in real earthquake systems [12]. It has been shown that the scaling found in such models is due to a spinodal in the limit of long-range stress transfer [13,14].

In the earthquake lattice models we use in this work we introduce inhomogeneities in the way that stress is dissipated. Stress is dissipated both at the lattice site of failure (site dissipation) and at neighboring sites which are damaged (damage dissipation). Spatial inhomogeneities are incorporated by varying this stress dissipation throughout the system in different spatial arrangements. We find that the scaling for damaged systems depends not only on the amount of damage, but also on the spatial distribution of that damage as well as the relation of the spatial damage or dissipation to the stress transfer range. Studying the effects of various spatial arrangements of site dissipation provides insights into how to construct a realistic model of an earthquake fault which is consistent with Gutenberg-Richter scaling.

## II. MODEL

We use a two-dimensional cellular automaton model of an earthquake fault which is a variant of the RJB model [15,16] and closely resembles the OFC model [11]. We begin with a two-dimensional lattice with periodic boundary conditions, where each site is either dead (damaged) or alive (active). Each

*racheledominguez@rmc.edu

 

live site $i$ contains an internal stress variable, $\sigma_i(t)$, which is a function of time. All stress variables are initially below a given threshold stress $\sigma^t$ and greater than or equal to a residual stress $\sigma^r$ (both of which we assume to be spatially homogeneous). Sites transfer stress to $z$ neighbors. Neighbors are defined as all sites within the transfer range $R$. Initially we randomly distribute stress to each site so that $\sigma^r < \sigma_i < \sigma^t$. We then increase the stress on all sites equally until one site reaches $\sigma^t$. At this point, the site at the threshold stress fails. When a site fails, some fraction of that site's stress, given by $\alpha_i(\sigma^t - \sigma^r \mp \eta)$, is dissipated from the system, where $\alpha_i$ is the site dissipation parameter ($0 \leqslant \alpha_i \leqslant 1$) which characterizes the fraction of stress dissipated from site $i$, and $\eta$ is a random flatly distributed noise. The stress of the site is lowered to $\sigma^r \pm \eta$ and the remaining stress is distributed equally to the site's $z$ neighbors.

To model more realistic faults, we use systems which are *damaged*, meaning they have both alive sites, which obey the rules outlined above, and dead sites, which do not hold any stress. Following Serino *et al.* [17], in addition to the stress dissipation regulated by the site dissipation parameter $\alpha_i$, we specify that any stress which is passed to a neighboring dead site also gets dissipated from the system. We can therefore regulate the spatial distribution of stress dissipation from the system with the distribution of the $\alpha_i$ and the placement of dead sites on the lattice. After the initial site failure, all live neighbors are then checked to see whether their stress has risen above $\sigma^t$. If it has, this site goes through the same failure procedure outlined above until all sites have stress below $\sigma^t$. The size of the avalanche is the number of failures that stem from the single initiating site. We refer to this whole avalanche process as a plate update.

Because stress is dissipated from the system both at the site of failure (as regulated by $\alpha_i$) and through dead sites which may be placed inhomogeneously throughout the system, we may think of each site $i$ as having a parameter which incorporates both types of dissipation, $\gamma_i = 1 - \phi_i(1 - \alpha_i)$, where $\phi_i$ is the fraction of live neighbors of site $i$. The mean value $\overline{\gamma} = \sum_i \gamma_i / N_a$, where $N_a$ is the number of live sites, is the average fraction of excess stress dissipated from the system per failed site.

We will want to compare the scaling in these systems with the scaling in simpler systems with no damage or with uniformly distributed damage. Klein *et al.* [9] studied the mean-field limit of OFC models with no damage and found that the number of avalanche events of size $s$ is associated with a spinodal critical point and obeys the scaling form

$$n(s) \sim e^{-\Delta h\, s^{\sigma}} / s^{\tau}, \tag{1}$$

where $\tau = 3/2$ and $\sigma = 1$. [Note that $n(s)$ is the number of events of size $s$, which is the noncumulative distribution, rather than the number of events of size $s$ or smaller, which is the cumulative distribution often discussed in relation to the Gutenberg-Richter law.] The quantity $\Delta h$ is a measure of the distance from the spinodal and vanishes as the dissipation parameter $\alpha \to 0$. In previous work [1,9], the authors have taken $\alpha_i = \alpha =$ constant. In this limit, Eq. (1) approaches a power law.

Serino *et al.* [1] showed that lattices with a spatially uniform distribution of damage also obey the scaling form of Eq. (1),

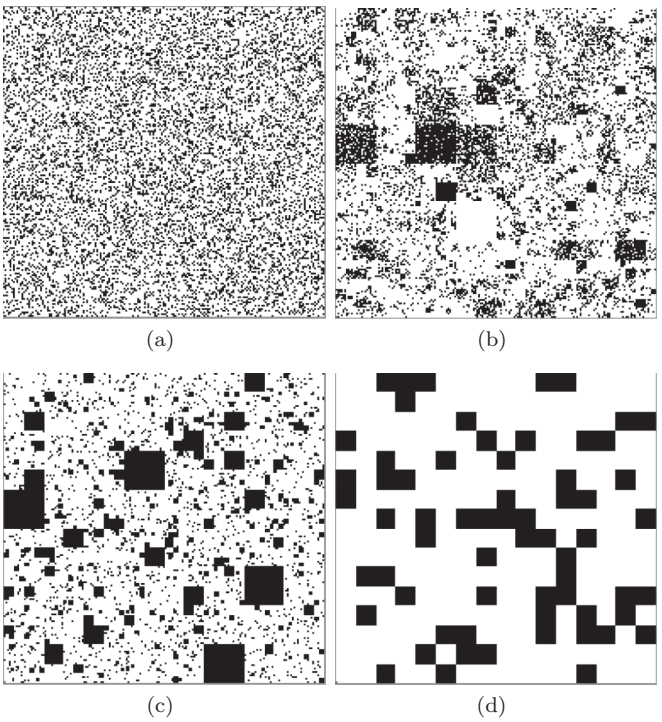


FIG. 1. Various configurations of 25% dead sites (in black) for lattices with linear size $L = 256$. Lattices contain (a) dead sites distributed randomly, (b) blocks of various linear sizes ranging from 1 to $L/8$, where each block has $p$ randomly distributed dead sites with $p$ varying for each block, (c) dead blocks of various sizes, (d) dead blocks of a single size $L/16$.

where $\Delta h$ also depends on $q$. In fact, long-range damaged systems with a fraction $\phi = 1 - q$ of live sites and constant site dissipation parameter $\alpha_i$ are equivalent to undamaged systems with site dissipation parameter $\alpha' = 1 - \phi(1 - \alpha)$. These systems approach the spinodal ($\Delta h \to 0$) as the total stress dissipation from the system vanishes: $\alpha' \to 0$. Physically, stress dissipation from the lattice system suppresses large avalanche events.

## III. QUALITATIVE BEHAVIOR OF SCALING

First we study the case with constant $\alpha_i = \alpha$ and damage distributed inhomogeneously throughout the system. In Fig. 1 we show two-dimensional lattices of linear size $L = 256$ and 25% of the sites dead. The lattices have various distributions of the dead sites, with various levels of spatial homogeneity. Figure 1(a) has the dead sites randomly distributed throughout the system. (In the long-range limit, this corresponds to homogeneous damage studied in Ref. [17].) Figures 1(b)– 1(d) incorporate clustering of dead sites to various degrees. The distribution of dead sites in Fig. 1(b) is set in the following way: Sublattices of the initial $256 \times 256$ lattice are considered with blocks of linear size $L/2^m$ with $3 \leqslant m \leqslant 8$. (The $m = 8$ case is just the initial $256 \times 256$ lattice with blocks of size 1.) With all sites initially alive, each of the largest blocks (of size $L/8$) is "damaged" with probability $p_b$. A block is damaged by killing each site within the block with probability $p_d$, which itself is drawn from a Gaussian distribution with center $c$ and width $w$. Then each undamaged block of linear size $L/16$

TABLE I. Averages and variances of $\gamma_i$ for the lattices and parameters given in Fig. 1 and for $R = 16$. The total number of dead sites is equal to 25% of the lattice for all distributions.

| Damage Distribution | $\overline{\gamma}$ | Variance |
|---|---|---|
| Fig. 1(a) | 0.2514 | $2.5 \times 10^{-4}$ |
| Fig. 1(b) | 0.2288 | $7.6 \times 10^{-3}$ |
| Fig. 1(c) | 0.2062 | $9.5 \times 10^{-3}$ |
| Fig. 1(d) | 0.1719 | $2.2 \times 10^{-2}$ |

is damaged with probability $p_b$ and so on until all of the undamaged blocks of size 1 are damaged with probability $p_b$. The parameters ($p_b$, $c$, and $w$) are varied until the final lattice has 25% damage. (The parameter choices are not unique for a particular fraction of damage.) Figure 1(c) has damage set in the same way, but with $p_d = 1$. Figure 1(c) has blocks of dead sites ("dead blocks") where the blocks also range in linear size from 1 to $L/8$.[1] Figure 1(d) has randomly distributed dead blocks with blocks of linear size of $L/16$ only. To characterize each configuration in Fig. 1, we calculate $\overline{\gamma}$ and the variance of $\gamma_i$ for an interaction range $R = 16$ and $\alpha_i = 0\,\forall i$. The results are summarized in Table I.

Figure 2 shows $n(s)$, the numerical distribution of avalanche events of size $s$, corresponding to the various distributions of damage in Fig. 1 for a stress transfer range of $R = 16$. Figure 2 also shows in black the best-fit lines of the data to Eq. (1). We use a weighted nonlinear least-squares method with four fitting parameters: $\tau$, $\Delta h$, $\sigma$, and an overall constant $n_0$. Fitting results are summarized in Table II. We note that the fit parameters are highly correlated with each other.

Figure 2 indicates that the scaling *form* of the data [Eq. (1)] remains the same in the presence of inhomogeneous damage, supporting the general paradigm explaining GR scaling in Ref. [1]. However, Serino *et al.* [1] found for systems with spatially uniform damage (where $\tau = 1.5$ and $\sigma = 1$) that $\Delta h = q^2$, where $q$ is the fraction of dead sites. This relationship clearly does not hold for the data in Fig. 2 since the lattices in Figs. 1(a)– 1(d) all have 25% damage but different distributions $n_s$, with different values of $\Delta h$ and $\sigma$. Therefore the scaling behavior of systems with damage depends not only on the total amount of damage to the system but also on the spatial distribution of damage. In particular, large events are suppressed more for lattices with damaged sites distributed more homogeneously. [Note that we do not expect finite-size scaling similar to that found in Ref. [1] because the values of $\sigma$ are different for the lattices of Figs. 1(a)–1(d).]

Because these lattices are identical in terms of size ($256 \times 256$), percentage of damaged sites (25%), and stress transfer range ($R = 16$), the differences in the large-event behavior are not due to the finite size of the lattice or the finite number of active sites in the lattice. Furthermore, the

[1]Lattices shown in Figs. 1(b) and 1(c) are constructed with a variety of length scales to reflect the fact that real fault systems are damaged on a variety of length scales. However, the distribution of lengths scales is arbitrary as the lattices in Fig. 1 are also constructed to show a qualitative range from spatially homogeneous to inhomogeneous damage distributions.

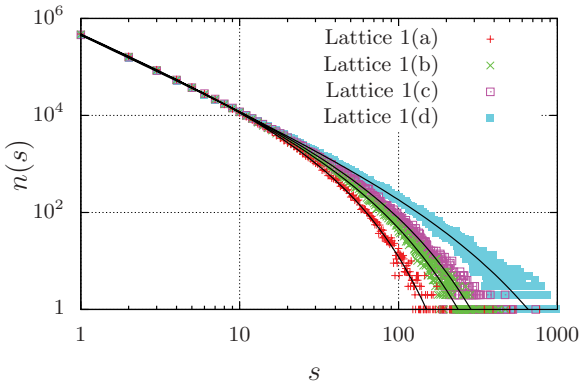


FIG. 2. (Color) Numerical distribution of avalanche events of size $s$ for various spatial distributions of dead sites. Data correspond to lattices and parameters given in Fig. 1 with stress transfer range $R = 16$. Black lines indicate the best fits of the data to Eq. (1). Final fit parameters of these lines are summarized in Table II.

results of Sec. III B indicate that the effect is due to the spatial distribution of $\gamma_i$ values and does not require any lattice damage. The calculated quantities in Table I would appear to indicate that the large-event suppression is correlated with both higher values of the average dissipation parameter $\overline{\gamma}$ and lower values of the variance of $\gamma$.

In order to better understand these results, we now study the effect of the interaction range relative to the length scales of inhomogeneities and the effect of clustering of dead sites.

### A. Length scales

For any given distribution of damage, the system will act as if the damage is homogeneous if the stress transfer range is long enough compared to the length scales of damage of the lattice. To illustrate the importance of relative length scales, we consider more lattices similar to Fig. 1(d) where there is a single length scale associated with damaged areas. In Fig. 3, we place blocks of damaged sites of linear size $b$ randomly in the system which has constant $\alpha_i = \alpha$. [Note that Fig. 1(d) is identical to Fig. 3(c).] All lattices shown in Fig. 3 have 25% dead sites and a linear system size of $L = 256$.

As we vary the ratio $R/b$, the measured value of $\overline{\gamma}$ varies from $\overline{\gamma} = \alpha$ for $R/b \ll 1$ to $\overline{\gamma} = 1 - \phi(1 - \alpha)$ for $R/b \gg 1$. In the former case, the live domains of the system appear nearly homogeneous with $\phi_i = 1$ except near the boundaries of dead blocks. The latter case is the limit of homogeneously

TABLE II. Summary of reduced $\chi^2$ values and final fit parameters corresponding to best-fit lines shown in black in Fig. 2. The data were fitted to the form $n(s) = n_0 \exp(-\Delta h s^\sigma)/s^\tau$ using a weighted nonlinear least-squares method. (Standard error for fit of parameters is smaller than the final significant figure given.)

| Damage Distribution | Reduced $\chi^2$ | $\tau$ | $\Delta h$ | $\sigma$ | $n_0$ |
|---|---|---|---|---|---|
| Fig. 1(a) | 1.21 | 1.47 | 0.0408 | 0.987 | $4.99 \times 10^5$ |
| Fig. 1(b) | 0.891 | 1.47 | 0.0569 | 0.821 | $4.97 \times 10^5$ |
| Fig. 1(c) | 0.979 | 1.49 | 0.0365 | 0.857 | $4.76 \times 10^5$ |
| Fig. 1(d) | 0.915 | 1.52 | 0.0299 | 0.719 | $4.61 \times 10^5$ |

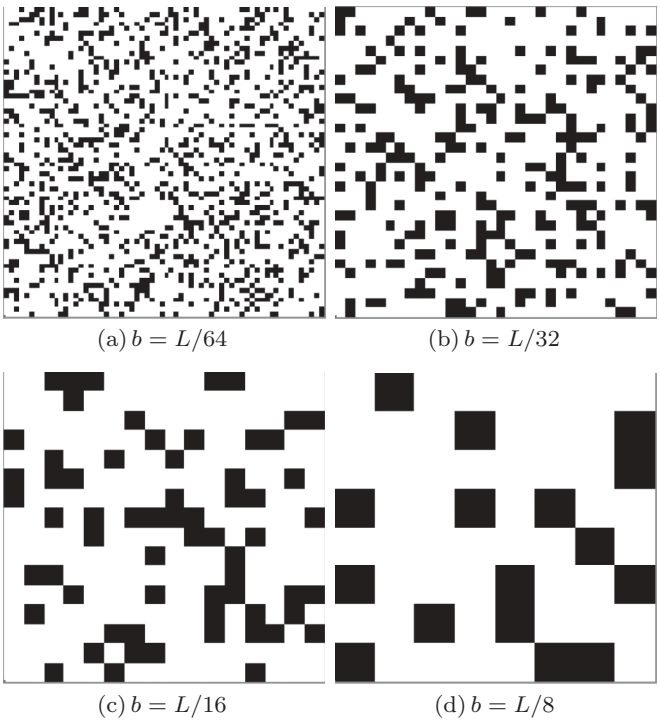


FIG. 3. Various configurations of 25% dead sites (in black) for a lattice with linear size $L = 256$. Each lattice has dead blocks of a single size $b$. Note that (c) is identical to Fig. 1(d).

distributed damage. In both limiting cases, the variance of $\gamma_i$ is small and the scaling is equivalent to the scaling for an undamaged system with $\alpha' = \overline{\gamma}$. In Fig. 4, we compare distributions $n_s$ for the lattice systems in Fig. 3 for $R = 16$ and $\alpha = 0$. As $R/b$ gets small, the values of $\overline{\gamma}$ also get small. The distribution $n_s$ of the corresponding data approaches a power law with the exponent $-3/2$ (shown in Fig. 4 as a solid red line) which is the form of the distribution of a system at the spinodal [see Eq. (1)]. The best-fit lines of the data to Eq. (1) are plotted in black. Fitting results are summarized in Table III.

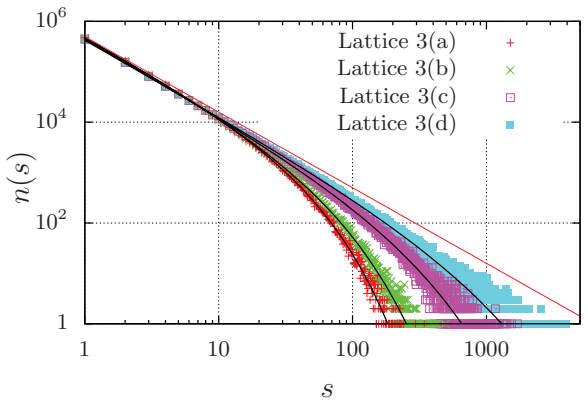


FIG. 4. (Color) Numerical distribution of avalanche events of size $s$ for lattices and parameters given in Fig. 3, and with stress transfer range $R = 16$. The straight red line $n_s \sim s^{-1.5}$ is drawn to show that the data are approaching a power law. Black lines indicate the best fits of the data to Eq. (1). Final fit parameters of these lines are summarized in Table III.

TABLE III. Summary of reduced $\chi^2$ values and final fit parameters corresponding to best-fit lines shown in black in Fig. 4. The data were fitted to the form $n(s) = n_0 \exp(-\Delta h s^\sigma)/s^\tau$ using a weighted nonlinear least-squares method. (Standard error for fit of parameters is smaller than the final significant figure given.)

| Damage Distribution | Reduced $\chi^2$ | $\tau$ | $\Delta h$ | $\sigma$ | $n_0$ |
|---|---|---|---|---|---|
| Fig. 3(a) | 1.03 | 1.47 | 0.0530 | 0.890 | $5.01 \times 10^5$ |
| Fig. 3(b) | 0.946 | 1.48 | 0.0588 | 0.801 | $5.00 \times 10^5$ |
| Fig. 3(c) | 0.915 | 1.52 | 0.0299 | 0.719 | $4.61 \times 10^5$ |
| Fig. 3(d) | 0.874 | 1.50 | 0.0216 | 0.644 | $4.30 \times 10^5$ |

### B. Spatial distributions of dissipation

The spatial distribution of damaged sites determines the spatial distribution of $\gamma_i$ values. A more direct way to control the numerical and spatial distributions of $\gamma_i$ is to use undamaged systems and vary the values of $\alpha_i$. In this way, we can isolate the effects of spatial redistribution of $\gamma_i$ values while holding the numerical distributions of $\gamma_i$ constant.

We construct three lattices, shown in Fig. 5, with site dissipation only; that is, they have no damage and $\gamma_i = \alpha_i$ for each system. The color in the figure indicates the values of $\alpha_i$. In Fig. 6, we show the numerical distributions of the $\alpha_i$ values $p(\alpha_i)$ for the three lattices. We see that the average value $\overline{\gamma} = 0.5$ for all three systems.

The lattices shown in Figs. 5(a) and 5(b) both have a uniform spatial distribution of $\alpha_i$ values. However, as shown in Fig. 6, the values of $\alpha_i$ for the lattice of Fig. 5(a) have a Gaussian distribution centered about $\alpha_i = 0.5$, while the values of $\alpha_i$ for the lattice of Fig. 5(b) have partial Gaussian distributions and are clustered near the values of $\alpha_i = 0$ and $\alpha_i = 1$. Thus, the variance of $\alpha_i$ values for lattice 5(a) is less than the variance for lattice 5(b). In Fig. 7 we present the numerical distributions of avalanche events, $n(s)$, for these systems when the stress transfer range is $R = 16$. We have fitted the data to Eq. (1), removing the data points $s \leqslant 5$ for the lattices of Figs. 5(b) and 5(c) [which do not fit the form of Eq (1)]. Fitting results are summarized in Table IV. Despite the different numerical distributions of $\alpha_i$ values, we see the distributions are similar

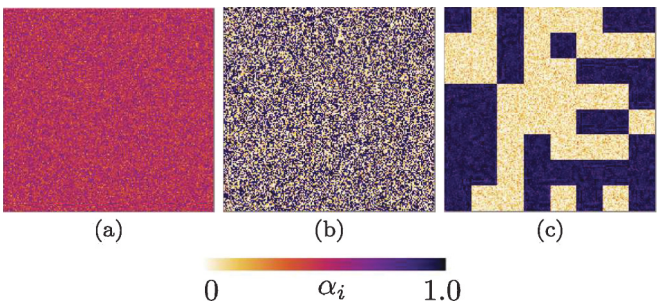


FIG. 5. (Color) Spatial arrangements of $\alpha_i$ values for three lattices with average value $\overline{\alpha} = 0.5$, no damage, and a linear system size of $L = 256$. Values of $\alpha_i$ are uniformly distributed in space for lattices (a) and (b). Lattice (c) has high (and low) values of $\alpha_i$ clustered into blocks of linear size $L/8$. Numerical distributions of $\alpha_i$ are shown in Fig. 6.

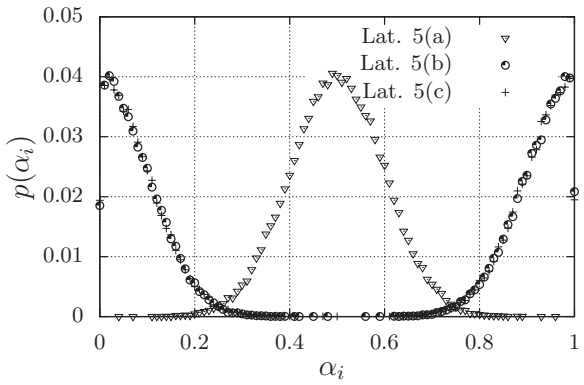


FIG. 6. Numerical distribution $p(\alpha_i)$ of site dissipation parameter values for lattices and parameters given in Fig. 5. Lattices in Figs. 5(b) and 5(c) have identical numerical distributions, while the lattice in Fig. 5(a) has approximately a Gaussian distribution centered about $\alpha_i = 0.5$.

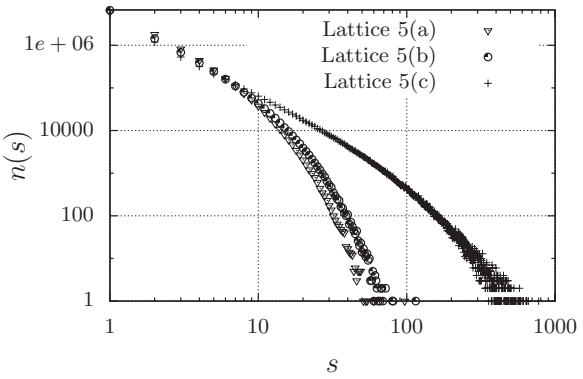


FIG. 7. Numerical distribution of avalanche events of size $s$ for lattices and parameters given in Fig. 5 and with stress transfer range $R = 16$. Numerical distributions of $\alpha_i$ values for these lattices are shown in Fig. 6.

for the lattices of Figs. 5(a) and 5(b), which both have spatially uniform distributions of $\alpha_i$ values.

However, the results for the lattice shown in Fig. 5(c) suggest that the spatial distribution of $\alpha_i$ has a robust effect on scaling, even when the averages and variances of $\alpha_i$ are the same. The lattices of Figs. 5(b) and 5(c) have nearly the same numerical distributions of $\alpha_i$ (Fig. 6), and therefore have the same value of the variance of $\alpha_i$. The spatial distributions of these two cases, however, are different: Lattice 5(a) has a uniform spatial distribution of $\alpha_i$ values, while lattice 5(c) has high (and low) $\alpha_i$ values clustered together into blocks of linear size $L/8 = 2R$. Despite having equal values of $\overline{\alpha_i}$ and equal variances of $\alpha_i$ values, lattice 5(c) experiences much larger events (by an order of magnitude.)

Evidently, the larger events depend crucially on the spatial clustering of low dissipation sites. This is because failing sites with low values of $\gamma_i$ pass along a high percentage of excess stress, encouraging the failure of neighboring sites. Thus, a large earthquake event is more likely to occur if the initial site of failure is well connected to a large number of sites with low dissipation parameters. In our system, connectedness is determined by spatial locality, so we require large clumps of sites with low values of $\gamma_i$ in order to allow for the occasional large earthquake event.

## IV. GUTENBERG-RICHTER SCALING

The Gutenberg-Richter scaling law states that the cumulative distribution of earthquake sizes is exponential in the magnitude [12]. In terms of the seismic moment, which has succeeded the Richter magnitude as the appropriate measure for earthquake sizes, the law may be reframed to state that the cumulative distribution of earthquake sizes, $N_M$, is a power law in the seismic moment, $M$ [1]:

$$N_M \sim M^{-\beta}, \quad \text{with} \quad \beta \equiv \frac{2b}{3}, \tag{2}$$

and $b$ is the so-called $b$ value of the Gutenberg-Richter law which has been measured for many real earthquake systems. The seismic moment $M$ is proportional to the size of the earthquake in this model [18]. Therefore, the relation appropriate for the systems considered in this work is the cumulative distribution of earthquake size:

$$N_s \sim s^{-\beta}, \tag{3}$$

or the corresponding noncumulative distribution

$$n_s \sim s^{-\tilde{\tau}}, \quad \text{with} \quad \tilde{\tau} = \beta + 1. \tag{4}$$

Serino *et al.* [1] construct a model for an earthquake fault system consisting of an aggregate of lattice models, where each lattice has a fraction $q$ of homogeneously distributed dead sites and $q$ varies from 0 to 1. The individual lattices have distributions consistent with Eq. (1), such that the pure power law is achieved only for a lattice with $q = 0$ corresponding to $\Delta h = 0$. The weighting factor $D_q$ gives the fraction of lattices with damage $q$. Considering the weighting factor to be constant with all values of $q$ contributing equally to the fault system, they find that the fault system obeys the scaling form

TABLE IV. Summary of reduced $\chi^2$ values and final fit parameters corresponding to best fits of data for large event sizes in Fig. 7 to the form $n(s) = n_0 \exp(-\Delta h s^\sigma)/s^\tau$ using a weighted nonlinear least-squares method. (Standard error for fit of parameters is smaller than the final significant figure given.) Fits use (at least) data points $s \geqslant 6$. We have reported a range of parameters because for the data points used, a range of fits yields reduced $\chi^2$ values between the values of 0.9 and 1.1.

| $\alpha$ Distribution | Reduced $\chi^2$ | $\tau$ | $\Delta h$ | $\sigma$ | $n_0$ |
|---|---|---|---|---|---|
| Fig. 5(a) | 0.619 | 1.49 | 0.188 | 0.997 | $7.50 \times 10^6$ |
| Fig. 5(b) | between 0.9 and 1.1 | $1.36 < \tau < 1.50$ | $0.176 > \Delta h > 0.128$ | $0.950 < \sigma < 1.02$ | $4.81 \times 10^6 < n_0 < 5.22 \times 10^6$ |
| Fig. 5(c) | between 0.9 and 1.1 | $1.45 < \tau < 1.64$ | $0.0945 > \Delta h > 0.0248$ | $0.677 < \sigma < 0.877$ | $2.83 \times 10^6 < n_0 < 3.35 \times 10^6$ |

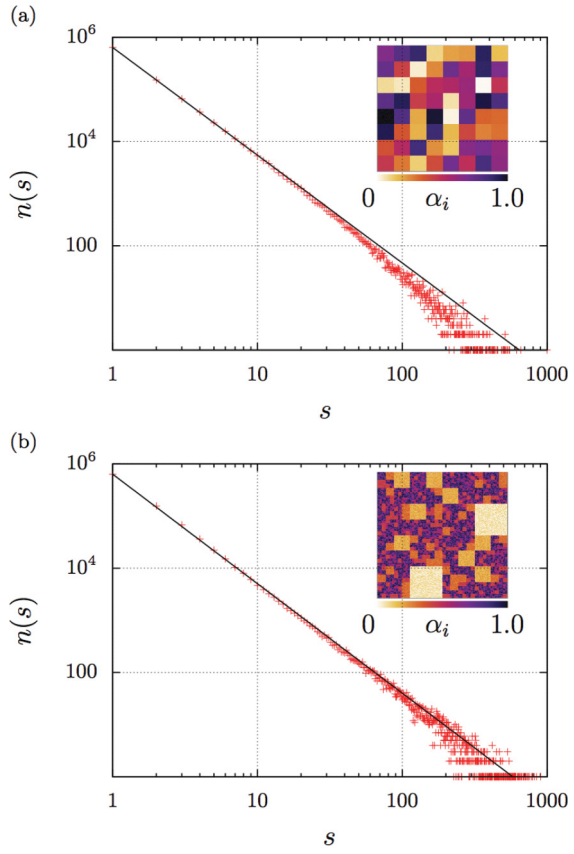


FIG. 8. (Color) Numerical distribution for avalanche events of size $s$ for systems with uniform numerical distributions for $\alpha_i$, but nonuniform spatial distributions of $\alpha_i$ which are shown in the insets. System size is $L = 512$ and stress transfer range is $R = 16$. Slopes of lines in red are (a) $\tilde{\tau} \simeq 2.07$ and (b) $\tilde{\tau} \simeq 2.10$.

of Eq. (4) with a value of $\tilde{\tau} = 2$. They also consider a power-law distribution of $D_q$ and fit the exponent to correspond to Gutenburg-Richter $b$ values found in real earthquake systems.

There are two important differences between the model considered by Serino *et al.* and our work: In the model treated by Serino *et al.*,

(1) the damage is distributed homogeneously;

(2) the individual lattices with homogeneous damage $q$ are noninteracting.

We investigate both the effect of the spatial arrangement of the damage and its relation to the stress transfer range as well as the effect of stress transfer between regions with different levels of damage.

We construct two lattice systems with a uniform numerical distribution of $\gamma_i$ which have scaling consistent with Serino *et al.*'s systems with constant distribution $D_q$. The first model essentially pieces together many homogeneous lattice systems: The numerical distribution of $\alpha_i$ values is uniform between 0 and 1, but spatially arranged into $N_B$ blocks of linear size $B$ [see Fig. 8(a) inset], where each block contains a random distribution of $\alpha_i$ values within an interval of size $1/N_B$. There are no dead sites, so that $\alpha_i = \gamma_i$. The effects of the boundaries between the blocks should be negligible if $B \ll R$. In Fig. 8(a), we present data from a system with $L = 512$, $R = 16$, and $B = 64$. The straight line shows the best fit to a power law with exponent $\tilde{\tau} \simeq 2.07$, which is consistent with the results for the aggregate lattice system of Serino *et al.* with $D_q = 1$.

We find that the size of the blocks, $B$, need not be the same for different values of $\alpha_i$. It is important that the boxes with lower values of $\overline{\gamma}$ be large enough to accommodate large avalanche events, but blocks with large $\alpha_i$ may be small because they are more likely to seed small avalanches. With this in mind we construct a lattice system with cascading length scales of blocks where the largest blocks have the lowest $\alpha_i$ values and decreasing sized blocks have increasing values of $\alpha_i$. The scaling results are shown in Fig. 8(b), where the red line drawn shows a power law with exponent $\tilde{\tau} \simeq 2.10$.

## V. CONCLUSIONS

We have studied both damage and site dissipation to inform the development of models of realistic earthquake faults with inhomogeneous stress dissipation. Spatially rearranging dead sites on a given lattice affects the numerical distributions of the effective stress dissipation parameters and the scaling behavior of large avalanche events, depending on the homogeneity of the damage and the length scales associated with the clustered dead sites. However, by studying site dissipation we find evidence suggesting that spatial distributions of dissipation parameters crucially affect scaling behavior even when the numerical distributions of dissipation parameters are the same.

The nonlinear fits to Eq. (1) (Tables II–IV) suggest that the scaling form remains the same in the presence of damage. In particular, the value of $\tau$, which is the scaling exponent associated with GR scaling, was found to be close to 1.5 for all systems investigated in this work. The importance of this result is that we have determined that the GR scaling exponent is not sensitive to the spatial distribution of damage. This suggests that the explanation for GR scaling developed in Ref. [1] also holds for systems with inhomogeneous damage.

However, the value of $\sigma$ deviates from 1 in our nonlinear fits for some systems. This poses new questions into the relationship between the parameter $\sigma$ and the largest earthquake events and suggests a new line of investigation into the relationship between the spatial structure of these events and other aspects of earthquake phenomenology. For example, lower values of sigma generated by nonrandom distributions of dead blocks, as seen in Fig. 1(d), are linked to an extended range of GR scaling behavior and an increased number of the largest events. Studies [19,20] have found that realistic damage rheologies can be related directly to the range of dynamics and variety of behaviors associated with earthquake faults. This includes such phenomena as characteristic earthquakes and accelerating seismic moment release. Here we find further evidence, using simple models of damage, that the pattern and type of damage can be directly related to the rate and magnitude of events at all sizes.

The models studied here go beyond those previously proposed by incorporating inhomogeneities with various spatial structures into the lattice and allowing areas with different

characteristic dissipation rates to interact. We stress again that our results are consistent with the paradigm proposed in Ref. [1] with no effect of the structure of the inhomogeneities on the GR scaling exponent.

**ACKNOWLEDGMENTS**

This work was funded by the DOE through Grant No. DE-FG02-95ER14498 and the NSERC and Aon Benfield/ICLR Industrial Research Chair in Earthquake Hazard Assessment.

[1] C. A. Serino, K. F. Tiampo, and W. Klein, Phys. Rev. Lett. **106**, 108501 (2011).
[2] W. Klein, J. B. Rundle, and C. D. Ferguson, Phys. Rev. Lett. **78**, 3793 (1997).
[3] P. Bak, C. Tang, and K. Wiesenfeld, Phys. Rev. Lett. **59**, 381 (1987).
[4] Hans Jacob S. Feder and J. Feder, Phys. Rev. Lett. **66**, 2669 (1991).
[5] D. Turcotte, Phys. Earth Planet. Inter. **111**, 275 (1999).
[6] G. Yakovlev, W. I. Newman, D. L. Turcotte, and A. Gabrielov, Geophys. J. Int. **163**, 433 (2005).
[7] K. F. Tiampo, J. B. Rundle, S. McGinnis, S. J. Gross, and W. Klein, Europhys. Lett. **60**, 481 (2002).
[8] K. F. Tiampo, J. B. Rundle, W. Klein, J. Holliday, J. S. SáMartins, and C. D. Ferguson, Phys. Rev. E **75**, 066107 (2007).
[9] W. Klein, H. Gould, N. Gulbahce, J. B. Rundle, and K. Tiampo, Phys. Rev. E **75**, 031114 (2007).
[10] R. Burridge and L. Knopoff, Bull. Seismol. Soc. Am. **57**, 341 (1967).
[11] Z. Olami, H. J. S. Feder, and K. Christensen, Phys. Rev. Lett. **68**, 1244 (1992).
[12] B. Gutenberg and F. Richter, Ann. Geophys. **9**, 1 (1956).
[13] J. B. Rundle and W. Klein, J. Stat. Phys. **72**, 405 (1993).
[14] W. Klein, M. Anghel, C. D. Ferguson, J. B. Rundle, and J. S. S. Martins, in *Geocomplexity and the Physics of Earthquakes* (American Geophysical Union, Washington, DC, 2000), AGU Monograph 120.
[15] J. B. Rundle and D. D. Jackson, Bull. Seismol. Soc. Am. **67**, 1363 (1977).
[16] J. B. Rundle and S. R. Brown, J. Stat. Phys. **65**, 403 (1991).
[17] C. A. Serino, W. Klein, and J. B. Rundle, Phys. Rev. E **81**, 016105 (2010).
[18] Edited by J. B. Rundle, D. L. Turcotte, and W. Klein, *Geocomplexity and the Physics of Earthquakes*, AGU Monograph 120 (American Geophysical Union, Washington, DC, 2000).
[19] V. Lyakhovsky, Y. Ben-Zion, and A. Agnon, J. Geophys. Res. **102**, 27635 (1997).
[20] Y. Ben-Zion and V. Lyakhovsky, Pure Appl. Geophys. **159**, 2385 (2002).